PHYSICAL REVIEW B **93**, 035207 (2016)

Intervalley scattering in hexagonal boron nitride

G. Cassabois, P. Valvin, and B. Gil*

Laboratoire Charles Coulomb (L2C), UMR 5221 CNRS-Université de Montpellier, F-34095, Montpellier, France

(Received 11 December 2015; published 28 January 2016)

We report photoluminescence experiments bringing the evidence for intervalley scattering in bulk hexagonal boron nitride. From a quantitative analysis of the defect-related emission band, we demonstrate that transverse optical phonons at the K point of the Brillouin zone assist inter-K valley scattering, which becomes observable because stacking faults in bulk hexagonal boron nitride provide a density of final electronic states. Time-resolved experiments highlight the different recombination dynamics of the phonon replicas implying either virtual excitonic states or real electronic states in the structural defects.

DOI: 10.1103/PhysRevB.93.035207

I. INTRODUCTION

Hexagonal boron nitride (hBN) is a nitride semiconductor with a very exotic crystalline phase, which is neither wurtzitic nor cubic, but a layered structure similar to graphite. Although optical measurements in high-quality samples suggested a direct band gap for bulk hBN [1], two-photon spectroscopy has recently allowed to elucidate the very peculiar optoelectronic properties of this indirect band-gap semiconductor [2]. In hBN, the extrema of the conduction and valence bands lie in different high-symmetry points, that are exceptionally *both* away from the Brillouin zone center [3–7]. In particular, it was shown that the emission lines above 5.7 eV (below 220 nm) consist in phonon replicas with an energy spacing reflecting the splitting of the different phonon branches in the middle of the Brillouin zone [2].

Bulk hBN displays an additional broad emission band below 5.7 eV, which originates from the presence of structural defects [8–11]. In a recent study combining cathodoluminescence measurements in a transmission electron microscope and *ab initio* calculations [11], several specific stacking faults have been identified within the broad defect-related emission band. However, the observation of sharp lines with a regular energy splitting, the so-called D lines, seems more likely to come from phonon-assisted processes rather than from an accidental periodical spacing of the stacking faults, which is not predicted by calculations [11]. In this paper, we address this issue by photoluminescence experiments under cw- and time-resolved-detection. From a quantitative analysis of the defect-related emission band, we demonstrate that transverse optical phonons at the K point of the Brillouin zone assist inter-K valley scattering, which becomes observable because stacking faults in bulk hBN provide a density of final electronic states. Time-resolved experiments highlight the different recombination dynamics of the phonon replicas implying either virtual excitonic states, or real electronic states in the structural defects.

II. EXPERIMENTS

Our experiments consist in photoluminescence (PL) spectroscopy in bulk hBN. Our sample is a commercial hBN crystal from HQ Graphene. In our experimental setup, the sample is hold on the cold finger of a closed-circle cryostat for temperature-dependent measurements from 10 K to room temperature. The excitation beam is provided by the fourth harmonic of a cw mode-locked Ti:Sa oscillator with a repetition rate of 82 MHz. The spot diameter is of the order of 300 μm with an excitation power of 20 and 400 μW in cw-detection and time-resolved measurements, respectively. An achromatic optical system couples the emitted signal to our two detection systems. For cw detection, the PL signal is dispersed in a $f = 500$ mm Czerny-Turner monochromator, equipped with a 300 grooves/mm grating blazed at 250 nm, and recorded with a back-illuminated CCD camera (Andor Newton 920), with a quantum efficiency of 50% at 210 nm, over integration times of 1 min. For time-resolved measurements, we use a $f = 500$ mm Czerny-Turner monochromator, equipped with a 1200 grooves/mm grating blazed at 400 nm, and a Hamamatsu streak camera (C10910) with one-hour acquisition times. For the defect-related emission band (from 220 to 240 nm) the streak camera was operated in the single-sweep mode, whereas for the weaker signal below 220 nm, the synchro-scan configuration is used in order to increase the signal-to-noise ratio.

In Fig. 1(a), we display the PL spectrum of hBN at 10 K, on a linear scale, over a 1 eV-spectral range centered at 5.5 eV. On the high-energy side, we observe the luminescence peak at 5.76 eV reported by Watanabe *et al.* in high-purity samples and attributed to the recombination of free excitons [1]. In the left inset of Fig. 1(a) showing a zoom of the PL spectrum around 5.8 eV, we see that the 5.76-eV emission line is a multiplet with fine structures extending over 40 meV, accompanied by a similar satellite band at 5.86 eV of lower intensity [9,10,12]. In our recent study by two-photon spectroscopy [2], we demonstrated that these lines, usually called S series in the literature, are in fact phonon replicas. hBN being an indirect band-gap semiconductor with a conduction (valence) band extremum at the M (K, respectively) point, radiative recombination must be assisted by emission of phonons of wave vector $\boldsymbol{MK}$ in order to fulfill momentum conservation [2]. The emission bands at 5.76 and 5.86 eV correspond to recombination assisted by optical and acoustic phonons, respectively. More specifically, the 5.76 eV emission band involves longitudinal and transverse optical phonons in the middle of the Brillouin zone, around T points, leading to the $X_{\mathrm{LO}(T)}$ and $X_{\mathrm{TO}(T)}$ phonon replicas [2]. Similarly, longitudinal and transverse acoustic phonons are associated to the $X_{\mathrm{LA}(T)}$ and $X_{\mathrm{TA}(T)}$ phonon replicas around

*bernard.gil@umontpellier.fr

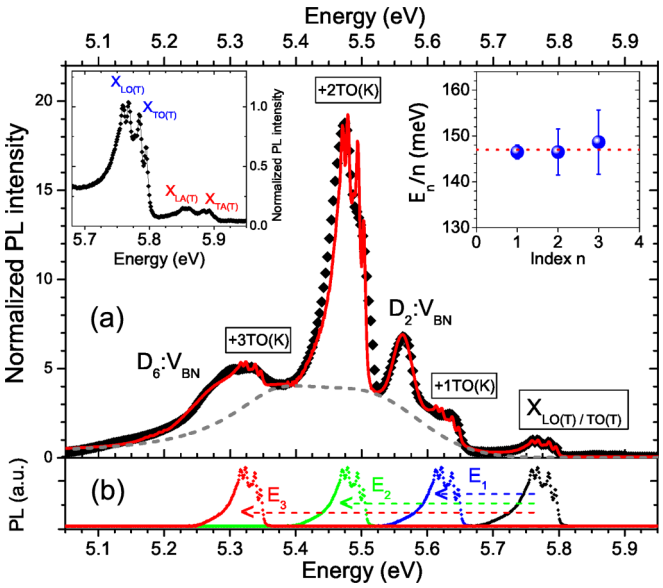

FIG. 1. (a) Normalized photoluminescence (PL) signal intensity in bulk hBN at 10 K, for an excitation at 6.3 eV (black diamonds), and fit (solid red line). The dashed gray line indicates the background signal intensity used in the fit, corresponding to the featureless defects emission in multiwalled boron nitride nanotubes (Ref. [14]). The D_2 and D_6 lines are attributed to the boron-nitride divacancy (V_{BN}). Right inset: energy shift E_n divided by the replica index n versus n. Left inset: zoom of the PL spectrum around 5.8 eV. (b) Emission spectrum of the $X_{\mathrm{LO}(T)/\mathrm{TO}(T)}$ line at 5.76 eV (black diamonds), and three replicas used in the fit in (a), obtained by a rigid energy shift of E_1 (blue diamonds), E_2 (green diamonds), and E_3 (red diamonds).

5.86 eV (Fig. 1, left inset). The fine structure observed for each replica remains an open question, zone-folding effects in multilayer segments of different thicknesses being one possible explanation [13]. Finally, we highlight that, in the phonon-assisted recombination process, the X_μ denomination of each replica (where μ is a phonon mode) can also be interpreted as referring to a *virtual* state, which lies at the energy of the emitted photon.

We now switch to the lower-energy part of the emission spectrum below 5.7 eV [Fig. 1(a)], which was identified as related to hBN defects by spatially-resolved cathodoluminescence measurements [8–11]. In contrast to the 5.76-eV emission line displaying a homogeneous spatial distribution of the emission intensity in hBN crystallites [8,9] and in few-layer hBN flakes [10,11], the defect-related emission bands below 5.7 eV display strong localization near dislocations and boundaries in cathodoluminescence measurements [8–11], with a striking spatial anti-correlation with the 5.76-eV PL line, as recently characterized with nanometric resolution in a transmission electron microscope [11]. Moreover, the emission spectrum below 5.7 eV exhibits various peaks at 5.62, 5.56, 5.47, and 5.3 eV, the so-called D lines [12], some of which may be attributed to phonon replicas on the basis of their regular spacing in the PL spectrum [8,14] but with puzzling variations of the emission intensity from one sample to another [15].

In the following, we show that the phonon cascade from the indirect exciton is not limited to one-phonon processes leading to the $X_{\mathrm{LA}(T)/\mathrm{TA}(T)}$ and $X_{\mathrm{LO}(T)/\mathrm{TO}(T)}$ lines, and that two-, three- and four-phonon-assisted recombination lines show up in the defect-related emission band around 5.5 eV. However, in contrast to the 5.86- and 5.76-eV lines associated to the virtual excitonic states $X_{\mathrm{LA}(T)/\mathrm{TA}(T)}$ and $X_{\mathrm{LO}(T)/\mathrm{TO}(T)}$, respectively, the phonon replicas in the D series are related to real electronic states provided by the structural defects. In other words, if the presence of defects or impurities in hBN leads to a broad emission spectrum between 5.1 and 5.7 eV, most of the D lines correspond to resonances of the phonon-assisted carrier relaxation rate.

III. INTERVALLEY SCATTERING

Our interpretation emanates from the full reconstruction of the PL spectrum [solid red line in Fig. 1(a)], going beyond the simple evaluation of the energy position of the different peaks, which is routinely performed in the literature. For that purpose we have developed a fitting procedure based on the following different elements: (i) the $X_{\mathrm{LO}(T)/\mathrm{TO}(T)}$ band and its replica shifted by an energy E_n where n is the replica index [as displayed in Fig. 1(b)] and multiplied by a factor a_n, (ii) an emission background [dashed gray line, Fig. 1(a)] accounting for the featureless defects emission observed in multiwalled boron nitride nanotubes [14], and (iii) two additional lines labeled D_2 and D_6, whose origin is not related to resonances of the phonon-assisted relaxation, but possibly to the boron-nitride divacancy (V_{BN}) as later discussed in the text. Although the phonon replicas of the $X_{\mathrm{LO}(T)/\mathrm{TO}(T)}$ band are obtained by a rigid shift, thus neglecting line-broadening and smoothing of the $X_{\mathrm{LO}(T)/\mathrm{TO}(T)}$ fine structures in these higher-order processes, we reach in Fig. 1(a) a striking fair agreement with the experimental data. The solid red line in Fig. 1(a) is obtained by taking $a_1 = 1.6$, $a_2 = 16.5$, and $a_3 = 1.5$, and two Gaussian lines with a central energy of 5.27 and 5.56 eV and a full width at half maximum of 83 ± 6 and 27 ± 2 meV for the D_6 and D_2 lines, respectively. From the ratio E_n/n of the energy shift and replica index plotted in the right inset of Fig. 1(a), we conclude that the phonons implied in the cascade from the $X_{\mathrm{LO}(T)/\mathrm{TO}(T)}$ virtual state have an energy of 147 ± 3 meV. Such an energy can be unambiguously assigned to the optical phonon of the TO branch at the K point of the Brillouin zone [16].

The implication of this particular mode in the phonon cascade stems from the symmetry properties of the hexagonal Brillouin zone of hBN. More specifically, in the reciprocal space, the ΓK distance does not only correspond to the distance from the center of the Brillouin zone to a K point, but also to the distance between adjacent K points ($\Gamma K = K'K$, where K' corresponds to an adjacent valley such that M is the middle of $[KK']$, as sketched in Fig. 2, inset). Denoting $\boldsymbol{q}$ the total wave vector carried by the emitted phonons, $\boldsymbol{q}$ is given by (i) $\boldsymbol{MK}$ for the $X_{\mathrm{LO}(T)/\mathrm{TO}(T)}$ and $X_{\mathrm{LA}(T)/\mathrm{TA}(T)}$ lines [2] (Fig. 2, left), and for higher-order processes, $\boldsymbol{q}$ is constant but decomposed into (ii) $\boldsymbol{MK' + K'K}$ for the 5.62-eV line involving one TO(K) optical phonon, (iii) $\boldsymbol{MK + KK' + K'K}$ for the 5.47-eV line involving two TO(K) optical phonons (Fig. 2, right), and (iv) $\boldsymbol{MK' + K'K + KK' + K'K}$ for the 5.32-eV line involving three TO(K) optical phonons. As a matter of fact, the phonon replicas observed in the defect-related emission band are the fingerprint for intervalley scattering

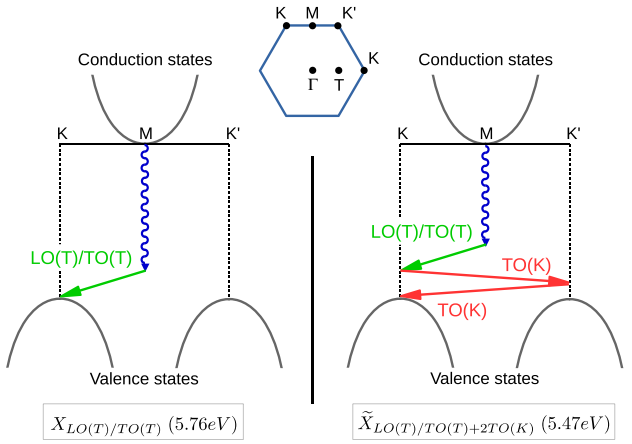

FIG. 2. Schematic representations, in the single-particle picture of the electronic band structure, of the phonon-assisted recombination processes of the $X_{\mathrm{LO}(T)/\mathrm{TO}(T)}$ line at 5.76 eV (left part), and of the $\widetilde{X}_{\mathrm{LO}(T)/\mathrm{TO}(T)+2\mathrm{TO}(K)}$ line at 5.47 eV (right part). Inset: top view of the first Brillouin zone with high-symmetry points. The green arrows correspond to the LO(T) or TO(T) phonons in the middle of the Brillouin zone, and the red arrows to the TO(K) phonons.

of carriers in hBN by emission of zone-edge TO(K) optical phonons.

Such a phenomenology is typical of indirect band-gap semiconductors such as germanium or silicon, where the many-valley picture of the band structure opens phonon-assisted scattering channels between the different valleys of the conduction band [17,18]. In the current case of bulk hBN, our measurements allow us to determine both the nature of the phonon and its wave vector. As far as the former is concerned, the explanation comes from the magnitude of the electron-phonon interaction, which is larger for optical phonons than for acoustic phonons [19]. In the specific case of direct band-gap crystals with inversion symmetry [20], phonon overtones are allowed only at high-symmetry points in the Brillouin zone, and for phonons belonging to degenerate representations and having different polarizations. In particular, overtones are always forbidden for longitudinal phonons, thus only leaving the possibility of transverse phonons. Since bulk hBN has inversion symmetry, and under the rough assumption that the symmetry of the $X_{\mathrm{LO}(T)/\mathrm{TO}(T)}$ virtual state is similar to the one of the fundamental exciton in direct band-gap semiconductors, one may expect only transverse optical phonons at K points to assist intervalley scattering, since the representations in hBN are degenerate at K points but not at M points. This is precisely the phenomenology observed in carbon nanotubes having a similar hexagonal structure, and for which inter-K valley scattering involve transverse optical phonon at K points [21,22]. In graphene also, the presence of the so-called D band in Raman spectra arises from a double-resonance configuration between adjacent K valleys involving TO phonons at K points [23]. We eventually point out the need for a proper group symmetry analysis of multiphonon overtones in bulk hBN, which is beyond the scope of this work, but still required for reaching a comprehensive understanding of high-order phonon scattering processes in this material.

TABLE I. The first column indicates the energy of the main emission lines in bulk hBN, the second one the standard labeling found in the literature, and the last column the nature of the phonon replica involving either virtual excitonic states (X_μ), or real ones ($\widetilde{X}_\mu$) due to the presence of defects in hBN. Boron-nitride divacancy (V_{BN}).

E (eV)	Label	Origin
5.86	$S_{1,2}$	$X_{\mathrm{LA}(T)/\mathrm{TA}(T)}$
5.76	$S_{3,4}$	$X_{\mathrm{LO}(T)/\mathrm{TO}(T)}$
5.62	D_1	$\widetilde{X}_{\mathrm{LO}(T)/\mathrm{TO}(T)+1\mathrm{TO}(K)}$
5.56	D_2	V_{BN}
5.47	$D_{3,4}$	$\widetilde{X}_{\mathrm{LO}(T)/\mathrm{TO}(T)+2\mathrm{TO}(K)}$
5.32	D_5	$\widetilde{X}_{\mathrm{LO}(T)/\mathrm{TO}(T)+3\mathrm{TO}(K)}$
5.27	D_6	V_{BN}

In Table I, we summarize our identification of the different emission lines in bulk hBN, which were simply called S and D series so far. The lines at 5.62 and 5.47 eV usually called D_1 and $D_{3,4}$ correspond to the phonon-assisted recombination lines $\widetilde{X}_{\mathrm{LO}(T)/\mathrm{TO}(T)+1\mathrm{TO}(K)}$ and $\widetilde{X}_{\mathrm{LO}(T)/\mathrm{TO}(T)+2\mathrm{TO}(K)}$, involving an optical phonon in order to reach the $X_{\mathrm{LO}(T)/\mathrm{TO}(T)}$ virtual excitonic state, plus 1 and 2 TO(K) phonons, respectively. Note that, for the phonon replicas emerging in the defect-related emission band, we use the $\widetilde{X}_\mu$ modified notation in order to highlight the fact that, in this case, *real* electronic states lie at the energy of the emitted photon in contrast to the $X_{\mathrm{LO}(T)/\mathrm{TO}(T)}$ phonon replica. As far as the $\widetilde{X}_{\mathrm{LO}(T)/\mathrm{TO}(T)+3\mathrm{TO}(K)}$ line is concerned, it appears to partly overlap with the donor-acceptor pair recombination line discussed in Refs. [24,25]. The multicomponent nature of the emission band around 5.3 eV can also be observed in other studies such as Ref. [10], where the donor-acceptor pair line clearly emerges at 5.27 eV in agreement with the value used in our fitting procedure for the D_6 line.

IV. BORON NITRIDE DIVACANCY

We now comment on the D_2 emission at 5.56 eV, which origin remains unclear, and that we tentatively attribute, together with the D_6 line (previously identified as a donor-acceptor pair transition [24]), to the optical transitions in a boron-nitride divacancy (V_{BN}) [26]. In Figs. 3(a) and 3(b), we display the temperature dependence of the PL spectrum from cryogenic to room temperature. All emission lines progressively broaden on raising the temperature, so that, at 290 K, the different transitions barely emerge upon the broad defect-related emission band [Fig. 3(b)]. However, we can notice that the D_2 emission is already hardly observable above 200 K, indicating a more pronounced variation with temperature and explaining its absence in studies performed at 150 K or above [11]. In order to quantitatively characterize this effect, we have analyzed the temperature dependence of each emission line, and in Fig. 3(c) we have plotted (on a log-log scale) the data in the three cases indicated by vertical dashed lines in Figs. 3(a) and 3(b), and corresponding to $X_{\mathrm{LO}(T)/\mathrm{TO}(T)}$ (5.76 eV), D_2 (5.56 eV), and $\widetilde{X}_{\mathrm{LO}(T)/\mathrm{TO}(T)+2\mathrm{TO}(K)}$ (5.47 eV). The D_2 band shows a completely different behavior compared to the other PL lines. Although the $X_{\mathrm{LO}(T)/\mathrm{TO}(T)}$ and $\widetilde{X}_{\mathrm{LO}(T)/\mathrm{TO}(T)+2\mathrm{TO}(K)}$ lines display some minor differences

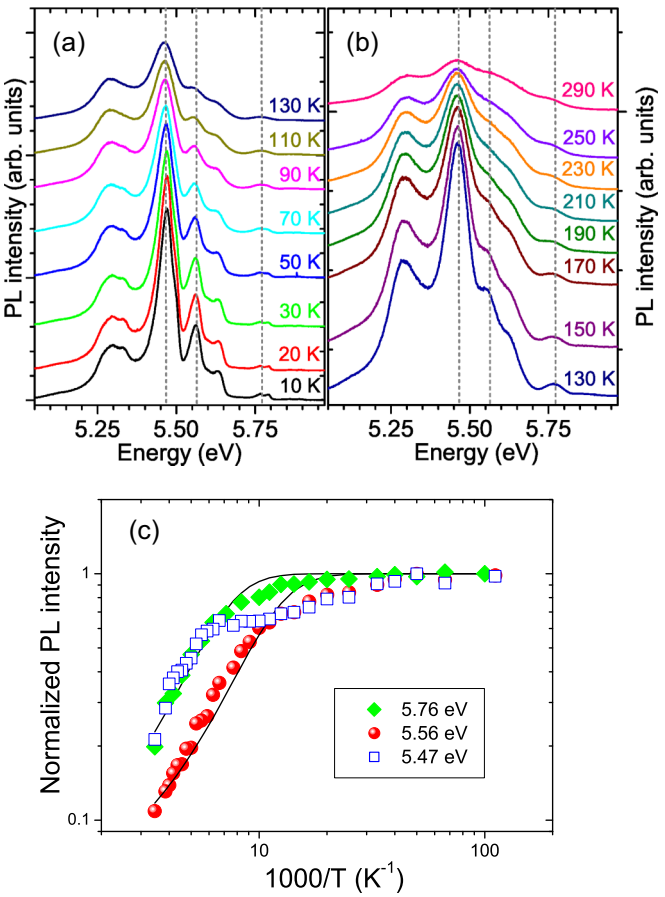

FIG. 3. Normalized photoluminescence (PL) signal intensity in bulk hBN for an excitation at 6.3 eV as a function of temperature, from 10 to 130 K (a) and from 130 to 290 K (b). (c) PL intensity versus 1000/T for three different emission bands indicated by vertical dashed lines in (a) and (b). Solid lines are Arrhenius fits with an activation energy E_a of 50 meV for the lines at 5.76 eV ($X_{\mathrm{LO}(T)/\mathrm{TO}(T)}$) and 5.47 eV ($\widetilde{X}_{\mathrm{LO}(T)/\mathrm{TO}(T)+2\mathrm{TO}(K)}$), and of 30 meV for the D_2 : V_{BN} line at 5.56 eV, possibly related to boron-nitride divacancy (V_{BN}).

below 100 K, we observe that, in a first approximation, a simple Arrhenius fit with an activation energy E_a of 50 meV [solid line in Fig. 3(c)] fairly reproduces their temperature variations. On the contrary, one has to take a smaller activation energy of 30 meV in the D_2 case, indicating a distinct nature compared to the various real- and virtual-phonon assisted processes. In Ref. [24], a similar conclusion was drawn for the D_6 line from PL excitation spectroscopy, concluding to the existence of donor-acceptor pair transitions.

The signature of defects in the optical response of hBN was investigated using many-body perturbation theory, in particular in Ref. [26] providing calculations of the optical absorption spectra in the cases of substitutional carbon, boron vacancy, nitrogen vacancy, and boron-nitride divacancy (V_{BN}). The excitonic band of V_{BN} is distinct from the other spectra as the divacancy possesses both acceptor and donor states in the vicinity of the band edges. More specifically, the transitions between acceptor and donor states in V_{BN} lead to absorption peaks approximately 0.8 eV below the direct exciton in hBN [26]. From the measurements of the indirect exciton energy at 5.95 eV [2] and the calculations of the indirect-direct gap splitting of 0.48 eV [7], one estimates the energy of donor-acceptor transitions in V_{BN} around 5.6 eV, fully consistent with the energy of the D_2 line. Moreover, the donor-acceptor transitions in V_{BN} display a fine structure with an intense high-energy component and a weaker 250 meV redshifted one [26], again fully consistent with the spectrum of the D_2 and D_6 lines, showing an energy splitting of 290 meV [Fig. 1(a)]. On the basis of our attribution of the D_2 and D_6 lines as being possibly related to donor-acceptor transitions in V_{BN}, we further interpret the anomalous temperature dependence of the D_2 signal intensity [Fig. 3(c)] as a thermally activated carrier redistribution within the electronic states of V_{BN}. Conversely, for the D_6 band corresponding to the V_{BN} donor-acceptor pair states lying at lowest energy, we observe the same variation of the signal intensity as for the other emission lines in hBN. Detailed investigation by means of local probe techniques will still be required in order to confirm that the D_6 and D_2 lines at 5.27 and 5.56 eV, respectively, originate from V_{BN}.

V. TIME-RESOLVED PHOTOLUMINESCENCE

Although the real- and virtual-phonon assisted transitions display a similar temperature-dependence of their PL signal intensity [Fig. 3(c)], and thus common nonradiative channels, we point out that the $\widetilde{X}_{\mathrm{LO}(T)/\mathrm{TO}(T)+n\mathrm{TO}(K)}$ transitions correspond to high-order processes in the phonon cascade from the fundamental indirect exciton. If all transitions were virtual, the higher the order of the electron-phonon interaction, the smaller the intensity of the PL signal. This is not the case in bulk hBN, precisely because structural defects give rise to a density of final electronic states, which is resonant for inter-K valley scattering via zone-edge TO(K) optical phonons. The existence of stacking faults in bulk hBN [11] thus makes possible the observation of inter-K valley scattering through a strong enhancement of the phonon-assisted relaxation rate which presents resonances at the $\widetilde{X}_{\mathrm{LO}(T)/\mathrm{TO}(T)+n\mathrm{TO}(K)}$ energies. As a matter of fact, at the spatial position of the stacking faults, inter-K valley scattering corresponds to an efficient nonradiative relaxation channel for the $X_{\mathrm{LO}(T)/\mathrm{TO}(T)}$ virtual state, which quenches the PL signal at 5.76 eV and seeds the one at lower energies, finally leading to a spatial anti-correlation of the corresponding cathodoluminescence maps [11]. In the temporal domain, the decay dynamics of the 5.76 eV signal becomes fast and dominated by nonradiative relaxation at the position of the stacking faults, where on the other hand, time-resolved PL measurements at the energy of the structural defects reveal their specific relaxation dynamics.

The efficient intervalley scattering on hBN stacking faults therefore decorrelates the PL decay dynamics of the virtual excitonic states ($X_{\mathrm{LA}(T)/\mathrm{TA}(T)}$ and $X_{\mathrm{LO}(T)/\mathrm{TO}(T)}$ lines at 5.86 and 5.76 eV, respectively) whose emission is observable in defect-free regions, from the PL decay dynamics of the real ones ($\widetilde{X}_{\mathrm{LO}(T)/\mathrm{TO}(T)+n\mathrm{TO}(K)}$ lines at 5.62, 5.47, and 5.32 eV for $n = 1$, 2, and 3, respectively), which is detected on stacking faults. In the following, we illustrate this point by time-resolved PL measurements which display a distinct phenomenology depending on the nature (virtual or real) of the phonon-assisted transitions.

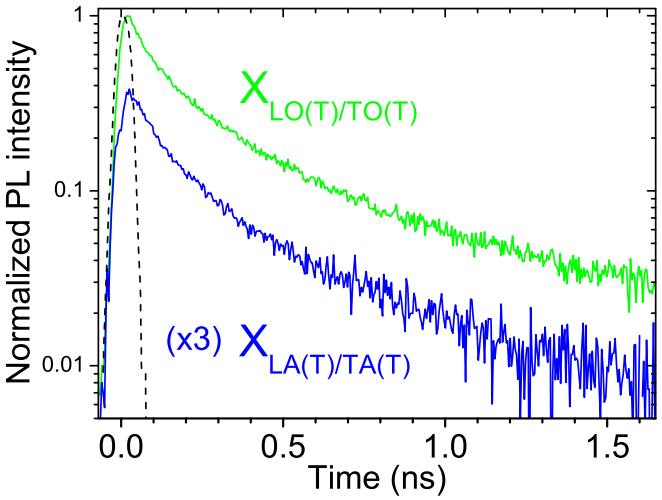

FIG. 4. Time-resolved photoluminescence (PL) in bulk hBN at 10 K, recorded at the energy of the $X_{LA(T)/TA(T)}$ and $X_{LO(T)/TO(T)}$ phonon replicas (left inset, Fig. 1) with identical time traces reflecting the decay of the indirect exciton reservoir (the acquisition time was three times larger for $X_{LA(T)/TA(T)}$), together with the system response function (dashed line).

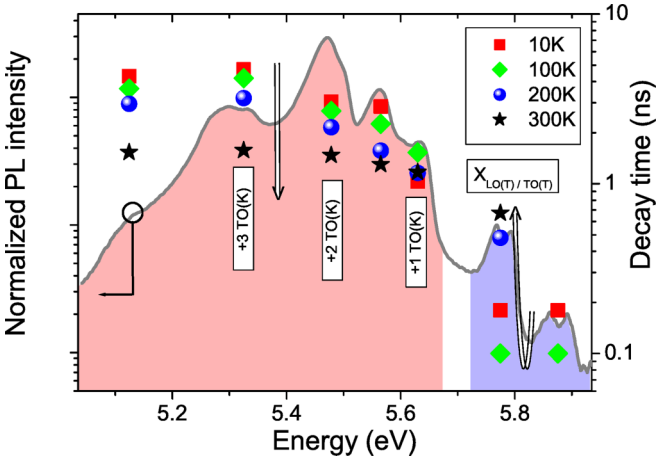

FIG. 5. Normalized photoluminescence (PL) signal intensity on a semilog scale (gray line, left axis) as a function of detection energy for an excitation at 6.3 eV at 10 K, and PL decay time $\tau_{1/e}$ on a semilogarithmic scale (symbols, right axis) as a function of detection energy for 10 K (red squares), 100 K (green diamonds), 200 K (blue circles), and 300 K (black stars). The red (blue) shaded area of the PL spectrum indicates the spectral domain of real (virtual)-phonon assisted transitions.

In the first case of virtual excitonic states ($X_{LA(T)/TA(T)}$ and $X_{LO(T)/TO(T)}$), the dynamics of the recombination processes leading to the PL emission at 5.86 and 5.76 eV reflects the global dynamics of the indirect exciton reservoir, and the temporal traces of the PL lines are expected to be the same [27]. We studied this by time-resolved experiments with unprecedented signal-to-noise ratio for the $X_{LA(T)/TA(T)}$ and $X_{LO(T)/TO(T)}$ lines (Fig. 4). While some studies have been devoted to time-resolved measurements focusing on the recombination of free excitons in hBN [9,15,28,29], there are diverse estimations for the decay time of the 5.76-eV line, with values of the order of either 60 ps [28] or 600–750 ps [9,29] at low temperature. Moreover, there is a single paper mentioning a decay time of 650 ps for the weaker 5.86-eV line [15]. We have carefully recorded the temporal traces of both $X_{LA(T)/TA(T)}$ and $X_{LO(T)/TO(T)}$ emission lines under femtosecond excitation at 6.3 eV. Our experiments provide the first simultaneous inspection of the 5.76 and 5.86-eV lines, and our data recorded over more than one decade allow us to identify the expected perfect similarity of the decay dynamics of the $X_{LA(T)/TA(T)}$ and $X_{LO(T)/TO(T)}$ lines (Fig. 4). In both cases, the time-resolved PL signal exhibits a biexponential decay with time constants of 130 ± 10 and 750 ± 10 ps, and amplitudes of 3.5 and 1, respectively. These time constants are in the range of the conflicting estimations mentioned before, and they are the signature for competing processes involved in the complex dynamics of the indirect exciton reservoir. However, complementary experiments are to be performed for clarifying the intrinsic or the extrinsic nature of the different relaxation processes revealed by the biexponential decay observed in our measurements.

While time-resolved measurements of the PL signal intensity at the energy of the $X_{LA(T)/TA(T)}$ and $X_{LO(T)/TO(T)}$ virtual states exhibit a biexponential decay (Fig. 4), the time traces are monoexponential (not shown) for the defect-related emission bands, with characteristic decay times of the order of few nanoseconds at 10 K (Fig. 5), in agreement with previous studies [9,15,28,29]. Note that the rise time of the PL temporal traces is beyond our temporal resolution of 20 ps, thus preventing any estimation of the intervalley scattering time but only giving an upper bound.

In Fig. 5, we display the summary of our temperature-dependent measurements, further highlighting the distinct recombination dynamics of the virtual and real phonon-assisted transitions. In order to perform the quantitative comparison shown in Fig. 5, we have plotted the PL decay time $\tau_{1/e}$ which is defined as the time needed for the signal to decrease by a factor e and which coincides with the relaxation time in the case of monoexponential decay. For the $\widetilde{X}_{LO(T)/TO(T)+2TO(K)}$ and $\widetilde{X}_{LO(T)/TO(T)+3TO(K)}$ transitions at 5.47 and 5.32 eV, we observe that the decay time decreases on raising the temperature, thus revealing the typical activation of nonradiative recombination processes, which drives the overall temperature-dependence of the recombination dynamics in the defect-related emission band (Fig. 5). Conversely, the $X_{LO(T)/TO(T)}$ transition at 5.76 eV displays a nonmonotonic behavior where the decay time $\tau_{1/e}$ first decreases down to 100 ± 10 ps at 100 K and then increases up to 670 ± 10 ps at room temperature (for the $X_{LA(T)/TA(T)}$ line, the PL signal is too weak above 100 K for performing time-resolved experiments and evidencing the expected increase of the decay time). Even though the small signal-to-background ratio at the 5.62 eV energy of the $\widetilde{X}_{LO(T)/TO(T)+1TO(K)}$ line partially masks its specific dynamics, our time-resolved experiments demonstrate opposite temperature dependencies for real and virtual phonon-assisted transitions, corresponding to the red and blue shaded areas in Fig. 5, respectively. In the spectral domain of the defect-related emission band which intensity is modulated by the resonant inter-K valley scattering, the recombination dynamics of the phonon replicas $\widetilde{X}_{LO(T)/TO(T)+nTO(K)}$ is governed by the physics of hBN defects, whereas at higher energy, the decay

of the $X_{\mathrm{LA}(T)/\mathrm{TA}(T)}$ and $X_{\mathrm{LO}(T)/\mathrm{TO}(T)}$ PL signals mirrors the dynamics of the indirect exciton reservoir.

The latter situation strongly differs from the standard configuration of direct excitons forming a quasiequilibrium system with an effective temperature [30], in which only the fraction of small-k excitons lying inside the light cone contributes to the PL signal, and which was proposed for hBN [29]. Although the effective dimensionality of excitons in hBN is still an open issue (either 3D or 2D?) questioning the validity of the former approach specific to 2D excitons, polaritonic effects observed in bulk semiconductors are also to be suppressed in hBN because of the indirect nature of the band gap. More generally, a key problem is to elucidate the fast decay of the indirect exciton reservoir on a subnanosecond time scale, which appears as the counterpart of the intense emission of hBN in high-purity crystals [1].

VI. CONCLUSIONS

In conclusion, we bring the evidence for intervalley scattering in bulk hBN by photoluminescence experiments. From a quantitative analysis of the defect-related emission band, we demonstrate that transverse optical phonons at the K point of the Brillouin zone assist inter-K valley scattering, which becomes observable because stacking faults in bulk hBN provide a density of final electronic states. We identify different emission lines of the so-called D series in bulk hBN as being phonon-assisted recombination lines involving up to three TO(K) phonons. We eventually illustrate the different recombination dynamics of the phonon replicas implying either virtual excitonic states, or real electronic states in the structural defects.

ACKNOWLEDGMENTS

We gratefully acknowledge D. Rosales, and C. L'Henoret for his technical support at the mechanics workshop. This work was financially supported by the network GaNeX (ANR-11-LABX-0014). GaNeX belongs to the publicly funded *Investissements d'Avenir* program managed by the French ANR agency. G.C. is a member of "Institut Universitaire de France."

[1] K. Watanabe, T. Taniguchi, and H. Kanda, Nat. Mater. **3**, 404 (2004).
[2] G. Cassabois, P. Valvin, and B. Gil, Nature Photonics (2016).
[3] Y.-N. Xu and W. Y. Ching, Phys. Rev. B **44**, 7787 (1991).
[4] J. Furthmüller, J. Hafner, and G. Kresse, Phys. Rev. B **50**, 15606 (1994).
[5] X. Blase, A. Rubio, S. G. Louie, and M. L. Cohen, Phys. Rev. B **51**, 6868 (1995).
[6] B. Arnaud, S. Lebègue, P. Rabiller, and M. Alouani, Phys. Rev. Lett. **96**, 026402 (2006).
[7] S.-P. Gao, Solid State Commun. **152**, 1817 (2012).
[8] P. Jaffrennou *et al.*, J. Appl. Phys. **102**, 116102 (2007).
[9] K. Watanabe *et al.*, Diam. Relat. Mater. **20**, 849 (2011).
[10] A. Pierret, J. Loayza, B. Berini, A. Betz, B. Plaçais, F. Ducastelle, J. Barjon, and A. Loiseau, Phys. Rev. B **89**, 035414 (2014).
[11] R. Bourrellier *et al.*, ACS Phot. **1**, 857 (2014).
[12] K. Watanabe and T. Taniguchi, Phys. Rev. B **79**, 193104 (2009).
[13] C. H. Lui and T. F. Heinz, Phys. Rev. B **87**, 121404 (2013).
[14] P. Jaffrennou, J. Barjon, T. Schmid, L. Museur, A. Kanaev, J.-S. Lauret, C. Y. Zhi, C. Tang, Y. Bando, D. Golberg, B. Attal-Tretout, F. Ducastelle, and A. Loiseau, Phys. Rev. B **77**, 235422 (2008).
[15] K. Watanabe and T. Taniguchi, Int. J. Appl. Cer. Tech. **8**, 977 (2011).
[16] J. Serrano, A. Bosak, R. Arenal, M. Krisch, K. Watanabe, T. Taniguchi, H. Kanda, A. Rubio, and L. Wirtz, Phys. Rev. Lett. **98**, 095503 (2007).
[17] N. O. Folland, Phys. Rev. B **1**, 1648 (1970).
[18] J. M. Tang, B. T. Collins, and M. E. Flatté, Phys. Rev. B **85**, 045202 (2012).
[19] *Fundamentals of Semiconductors*, edited by P. Y. Yu and M. Cardona (Springer-Verlag, Berlin Heidelberg, 1996).
[20] M. Hulin, Phys. Status Solidi **21**, 607 (1967).
[21] O. N. Torrens, M. Zheng, and J. M. Kikkawa, Phys. Rev. Lett. **101**, 157401 (2008).
[22] R. Matsunaga, K. Matsuda, and Y. Kanemitsu, Phys. Rev. B **81**, 033401 (2010).
[23] C. Thomsen and S. Reich, Phys. Rev. Lett. **85**, 5214 (2000).
[24] L. Museur and A. Kanaev, J. Appl. Phys. **103**, 103520 (2008).
[25] L. Museur, E. Feldbach, and A. Kanaev, Phys. Rev. B **78**, 155204 (2008).
[26] C. Attaccalite, M. Bockstedte, A. Marini, A. Rubio, and L. Wirtz, Phys. Rev. B **83**, 144115 (2011).
[27] S.-K. Lee, B.-J. Kwon, Y.-H. Cho, H.-J. Ko, and T. Yao, Phys. Rev. B **84**, 205216 (2011).
[28] K. Watanabe, T. Taniguchi, T. Kuroda, and O. Tsuda, Diam. Relat. Mater. **17**, 830 (2008).
[29] X. K. Cao, B. Clubine, J. H. Edgar, J. Y. Lin, and H. X. Jiang, Appl. Phys. Lett. **103**, 191106 (2013).
[30] A. V. Paraskevov, J. Lumin. **132**, 2913 (2012).